ANALYSIS OF MECHANISMS FOR THE CYCLIC CLEAVAGE OF WATER BY VISIBLE LIGHT

MEI HSU DUNG and JOHN J. KOZAK

Department of Chemistry and Radiation Laboratory, University of Notre Dame, Notre Dame, IN 46556 (U.S.A.)

(Received December 8, 1980; in revised form February 3, 1981)

Summary

The cyclic cleavage of water by visible light via coupled redox catalysts in colloidal systems has recently been reported by Grätzel and coworkers. In this paper we present an in-depth analysis of a mechanism for the consequent production of hydrogen and oxygen, focusing on the factors which may affect the stability of the photostationary state, the enhancement in the kinetics due to the presence of colloidally dispersed noble metal (oxides) and the sensitivity of the yield to the system parameters (intensity and illumination of the source). Emphasis is placed on comparison with the experimental data reported for the production of hydrogen and oxygen. The analysis and, especially, our simulations show that the underlying coupled chemical network, when triggered by the absorption of light, behaves as a true synergetic system, *e.g.* increasing the efficiency of the reactions via the introduction of a colloidally dispersed catalyst enhances the effect of increasing the intensity of the radiation source. Our simulations show that there may be an upper limit on the effectiveness of this synergetic effect in producing hydrogen and oxygen via a cyclic water cleavage reaction.

1. Introduction

Recently considerable attention has been directed toward the goal of finding chemical processes capable of facilitating the storage and transfer of light energy [1]. For example, with respect to the design and operation of photogalvanic cells, Albery and coworkers [2, 3] have studied a certain class of photoredox system in which a one-electron redox couple reacts with a two-electron redox couple; their mechanistic studies on the reaction of an organic dye redox couple (thionine) with an inorganic redox couple (Fe(II)–Fe(III)) and the earlier study of Albery and Archer [4] provide valuable insights into the factors involved in optimizing the efficiency of such photogalvanic systems. A quite different class of light-processing system has been developed recently which is capable of achieving hydrogen [5 - 8] and

0047-2670/81/0000-0000/$02.50

oxygen [9] production from water by visible light using coupled redox catalysts in the presence of certain colloids. In a particularly intriguing recent study, Kalyanasundaram and Grätzel [10] have demonstrated that a system of two redox catalysts in the presence of noble metal (oxide) dispersions can effect the cyclic cleavage of water into hydrogen and oxygen by visible light. It will be this class of systems, and in particular the study of Kalyanasundaram and Grätzel, that will be the primary focus of the present contribution.

From a "synergetic" point of view both photogalvanic cells and water cleavage systems involve coupled chemical networks which are triggered into action via the absorption of electromagnetic (or ionizing [11]) radiation. This point of view suggests that a common theoretical approach can be taken to address questions of stability, optimization and the relative efficiency of these energy storage and transfer systems; in particular, the methods of non-equilibrium thermodynamics [12], non-linear kinetics [13] and synergetics [14] provide a basis for carrying out such a study. A first step in this program, a stability analysis of photochemical mechanisms for photogalvanic cells, has been reported recently [15]. In the present study this approach is extended to the analysis of water cleavage systems with particular emphasis on the photoinduced cyclic water cleavage experiment described in ref. 10.

The system discovered by Kalayanasundaram and Grätzel is outlined in Fig. 1. Using $S \equiv Ru(bipy)_3^{2+}$, $S^+ \equiv Ru(bipy)_3^{3+}$, $A = MV^{2+}$ and $A^- \equiv MV^+$ (bipy ≡ bipyridine; $MV^{2+} \equiv$ methyl viologen), the following sequence of reactions provides a first approximation to the underlying chemical network:

$$S \xrightarrow{h\nu} S^* \xrightarrow{k_0} S \tag{1a}$$

$$S^* + A \xrightarrow{k_1} S^+ + A^- \tag{1b}$$

$$S^+ + A^- \xrightarrow{k_2} S + A \tag{1c}$$

$$S^+ + \tfrac{1}{2}H_2O \xrightarrow{k_3} S + H^+ + \tfrac{1}{4}O_2\uparrow \tag{1d}$$

$$A^- + H_2O \xrightarrow{k_4} A + OH^- + \tfrac{1}{2}H_2\uparrow \tag{1e}$$

The overall mechanism described by eqns. (1a) - (1e) will be referred to in our later discussions as mechanism (I). It is in steps (1d) and (1e) that the colloidally dispersed noble metal (oxide) fulfills its role as a kind of micro-electrode on which the catalytic cleavage of water takes place.

Our analysis of mechanism (I) is organized in the following way. Since the production of hydrogen and oxygen is most easily controlled under steady state conditions, we investigate the existence properties and stability properties of the photostationary state, using first the methods of linear stability theory (Section 2) and then the methods of thermodynamic stability theory (Section 3). After reviewing the available kinetic rate data, we report in Section 4 the results of representative time evolution studies in which

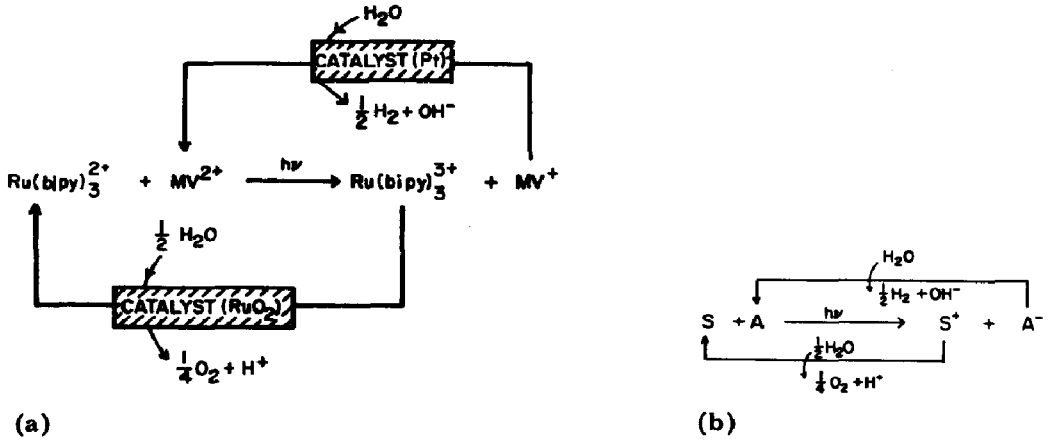

Fig. 1. Schematic diagrams of the cyclic water cleavage system.

such factors as light intensity and rate enhancement due to microelectrode catalysis are assessed. In Section 5 we consider explicitly the production of hydrogen and oxygen under steady state conditions; our simulations corroborate the experimental findings reported in ref. 10. This point may be of some importance inasmuch as it has been noted that the original report of Kalayanasundaram and Grätzel has been questioned by other workers who have repeated the experiment and have failed to obtain results similar to those reported in ref. 10. At the very least, the present study suggests regions of parameter space that might be explored to enhance the production of hydrogen and oxygen. The final section is devoted to a short discussion of the possible importance of electrostatic factors in water cleavage reactions.

2. Linear stability analysis of the steady state

Corresponding to the general mechanism, eqns. (1a) - (1e), we may write down the evolution equations of the problem:

$$\frac{d[S^*]}{dt} = g[S] - k_0[S^*] - k_1[S^*][A] \equiv M \tag{2}$$

$$\frac{d[S]}{dt} = -g[S] + k_0[S^*] + k_2[S^+][A^-] + k_3[S^+] \equiv P \tag{3}$$

$$\frac{d[S^+]}{dt} = k_1[S^*][A] - k_2[S^+][A^-] - k_3[S^+]$$

$$\frac{d[A]}{dt} = -k_1[S^*][A] + k_2[S^+][A^-] + k_4[A^-] \equiv Q \tag{4}$$

$$\frac{d[A^-]}{dt} = k_1[S^*][A] - k_2[S^+][A^-] - k_4[A^-]$$

Given that the system is closed with respect to mass transport, we have the following conservation conditions:

$$[S^*] + [S] + [S^+] = [S^*]_i + [S]_i + [S^+]_i = a \tag{5}$$

$$[A] + [A^-] = [A]_i + [A^-]_i = b \tag{6}$$

where a and b are constants and the subscript i denotes the initial concentration of the component considered; in eqns. (2) and (3) g refers to the light flux coefficient.

Under steady state conditions the right-hand side of each of eqns. (2) - (4) vanishes; thus, we have

$$g[S]_0 - k_0[S^*]_0 - k_1[S^*]_0[A]_0 = 0 \tag{7}$$

$$-g[S]_0 + k_0[S^*]_0 + k_2[S^+]_0[A^-]_0 + k_3[S^+]_0 = 0 \tag{8}$$

$$-k_1[S^*]_0[A]_0 + k_2[S^+]_0[A^-]_0 + k_4[A^-]_0 = 0 \tag{9}$$

where the subscript 0 denotes the steady state concentration of the particular species. Using the conservation conditions, eqns. (5) and (6), we may solve these algebraic equations for the concentration $[A]_0$ of electron acceptor at the steady state; in particular, the possible concentrations of $[A]_0$ are the null solutions of the equation

$$f([A]) = -k_1[A]g\{k_3a - k_4(b - [A])\} + k_2k_4(b - [A])^2(k_0 + k_1[A] + g) + k_4(b - [A])(k_0 + k_1[A] + g)$$

The function $f([A])$ has the following limiting properties:

$$\lim_{[A] \to \infty} f([A]) > 0$$

$$\lim_{[A] \to -\infty} f([A]) < 0$$

$$\lim_{[A] \to 0} f([A]) = k_2k_4b^2(k_0 + g) + k_4b(k_0 + g) > 0$$

$$\lim_{[A] \to b} f([A]) = -k_1bgk_3a$$

We display in Fig. 2 a (qualitative) sketch of this functional behavior. From this sketch it is evident that there is only one root, $[A]_0$, of the equation lying between $[A] = 0$ and $[A] = b$ (where, again, the constant b is the upper bound on the overall concentration of species A (see eqn. (6))).

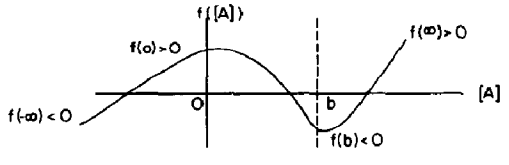

Fig. 2. A sketch of the function $f([A])$ *vs.* $[A]$ (see text).

Before proceeding it is necessary to ensure that the following bounds are satisfied by the steady state concentrations $[A^-]_0$ and $[S]_0$, $[S^*]_0$, $[S^+]_0$:

$$0 \leqslant [A^-]_0 \leqslant b \tag{10}$$

$$0 \leqslant [S]_0, [S^*]_0, [S^+]_0 \leqslant a \tag{11}$$

The first inequality follows directly from the condition $0 \leqslant [A]_0 \leqslant b$ and the conservation condition, eqn. (6). From eqns. (8) and (9) we have

$$\begin{aligned} k_3[S^+]_0 &= k_3(a - [S]_0 - [S^*]_0) \\ &= k_4(b - [A]_0) \end{aligned}$$

Using the relation for $[S^*]_0$ derived from eqn. (7), this equation becomes

$$\begin{aligned} [S]_0 &= \frac{k_0 + k_1[A]_0}{k_0 + k_1[A]_0 + g}\left\{a - \frac{k_4}{k_3}(b - [A]_0)\right\} \\ &\leqslant \frac{k_0 + k_1[A]_0}{k_0 + k_1[A]_0 + g} a \leqslant a \end{aligned}$$

Also

$$\begin{aligned} [S^*]_0 &= \frac{g}{k_0 + k_1[A]_0 + g}\left\{a - \frac{k_4}{k_3}(b - [A]_0)\right\} \\ &\leqslant \frac{g}{k_0 + k_1[A]_0 + g} a \leqslant a \end{aligned}$$

and

$$\begin{aligned} [S^+]_0 &= a - [S]_0 - [S^*]_0 \\ &= \frac{k_4(b - [A]_0)}{k_3} \geqslant 0 \end{aligned}$$

Further, from eqn. (9) we have

$$[S^*]_0 = \frac{1}{k_1[A]_0}\{k_2[S^+]_0(b - [A]_0) + k_4(b - [A]_0)\} \geqslant 0$$

and from eqn. (8) we have

$$[S]_0 = \frac{1}{g}(k_0[S^*]_0 + k_1[S^*]_0[A]_0) \geqslant 0$$

Finally, noting that

$$2a \geqslant [S]_0 + [S^*]_0 \geqslant 0$$

and using the conservation condition, eqn. (5), we are guaranteed that $[S^+]_0 \leqslant a$, which completes the proof of relation (11).

The stability analysis is carried out by linearizing eqns. (2) - (4) about the steady state and constructing the variational equation

$$\frac{\mathrm{d}}{\mathrm{d}t}\begin{bmatrix}\delta[\mathrm{S}^*]\\ \delta[\mathrm{S}]\\ \delta[\mathrm{A}]\end{bmatrix} = \begin{bmatrix}M_{\mathrm{S}^*} & M_{\mathrm{S}} & M_{\mathrm{A}}\\ P_{\mathrm{S}^*} & P_{\mathrm{S}} & P_{\mathrm{A}}\\ Q_{\mathrm{S}^*} & Q_{\mathrm{S}} & Q_{\mathrm{A}}\end{bmatrix}\begin{bmatrix}\delta[\mathrm{S}^*]\\ \delta[\mathrm{S}]\\ \delta[\mathrm{A}]\end{bmatrix} \tag{12}$$

where

$$M_{\mathrm{S}^*} = -k_0 - k_1[\mathrm{A}]_0 \equiv -k_0 - \eta$$

$$M_{\mathrm{S}} = g$$

$$M_{\mathrm{A}} = -k_1[\mathrm{S}^*]_0 \equiv -\alpha$$

$$P_{\mathrm{S}^*} = k_0 - k_2(b - [\mathrm{A}]_0) - k_3 \equiv k_0 - \beta - k_3$$

$$P_{\mathrm{S}} = -g - k_2(b - [\mathrm{A}]_0) - k_3 \equiv -g - \beta - k_3$$

$$P_{\mathrm{A}} = -k_2(a - [\mathrm{S}]_0 - [\mathrm{S}^*]_0) \equiv -\gamma$$

$$Q_{\mathrm{S}^*} = -k_1[\mathrm{A}]_0 - k_2(b - [\mathrm{A}]_0) \equiv -\eta - \beta$$

$$Q_{\mathrm{S}} = -k_2(b - [\mathrm{A}]_0) = -\beta$$

$$Q_{\mathrm{A}} = -k_1[\mathrm{S}^*]_0 - k_2(a - [\mathrm{S}]_0 - [\mathrm{S}^*]_0) - k_4 \equiv -\alpha - \gamma - k_4$$

In these defining relations the constants α, β, γ and η are positive quantities. The stability of system (I) at the steady state is inferred by determining the eigenvalues $\{\lambda_1, \lambda_2, \lambda_3\}$ of the matrix

$$\begin{bmatrix}M_{\mathrm{S}^*} & M_{\mathrm{S}} & M_{\mathrm{A}}\\ P_{\mathrm{S}^*} & P_{\mathrm{S}} & P_{\mathrm{A}}\\ Q_{\mathrm{S}^*} & Q_{\mathrm{S}} & Q_{\mathrm{A}}\end{bmatrix}$$

The characteristic equation corresponding to this determinant is

$$\lambda^3 + a_2\lambda^2 + a_1\lambda + a_0 = 0 \tag{13}$$

where

$$a_2 = k_0 + \eta + g + \beta + k_3 + \alpha + \gamma + k_4 > 0$$

$$a_1 = k_0\beta + k_0k_3 + k_0\alpha + k_0\gamma + k_0k_4 + \eta g + \eta\beta + \\ + \eta k_3 + g\alpha + g\gamma + gk_4 + \beta k_4 + k_3\alpha + k_3\gamma + \\ + k_3k_4 + \eta\gamma + \eta k_4 + g\beta + gk_3 \\ > 0$$

and

$$a_0 = k_0\beta k_4 + k_0k_3\alpha + k_0k_3\gamma + k_0k_3k_4 + \eta gk_4 + \\ + \eta\beta k_4 + \eta k_3\gamma + \eta k_3k_4 + g\beta k_4 + gk_3\alpha + gk_3\gamma + gk_3k_4 \\ > 0$$

Given the signs of the coefficients $\{a_1, a_2, a_3\}$, the roots of the characteristic equation, eqn. (13), are either (1) three real roots, all negative, or (2) one real root which is negative and a pair of complex conjugates. If the three eigenvalues of the characteristic equation are all real and negative (the first possibility), the asymptotic stability of the steady state is guaranteed. If the second possibility is realized, a small perturbation from the steady state will result in a damped oscillatory decay back to the steady state. This conclusion may be demonstrated explicitly in the special case where the rate constants k_3 and k_4 are of comparable magnitude. In particular, when $k_3 = k_4$ one eigenvalue will be $\lambda_3 = -k_3$ and the sum and product of the other two eigenvalues λ_1 and λ_2 are (setting $\chi = \gamma + \alpha + g + \lambda$)

$$\lambda_1 + \lambda_2 = -(k_0 + \eta + \alpha + g + \chi)$$

$$\lambda_1\lambda_2 = k_0\chi + \eta g + \eta\chi + \alpha g + g\chi + \alpha k_0$$

Then, if

$$\Delta = (\lambda_1 + \lambda_2)^2 - 4\lambda_1\lambda_2$$

$$= (g + k_0 - \eta - \alpha - \chi)^2 - 4\eta\chi + 4k_0\eta$$

is positive, the two roots (λ_1, λ_2) will be real and negative (guaranteeing asymptotic stability of the steady state), whereas if $\Delta < 0$ the two roots (λ_1, λ_2) will be a complex conjugate pair (with evolution back to the steady state from a perturbed configuration characterized by a damped oscillatory decay).

This analysis was carried out assuming that the linearized form of Beer's law was adequate to characterize the radiation flux contribution to the evolution equations eqns. (2) - (4). However, the analysis is completed with no complications if the full Beer's law expression for the flux is used. In particular, we write the evolution equations in the more general form

$$\frac{d[S^*]}{dt} = I - k_0[S^*] - k_1[S^*][A] \equiv M \tag{14}$$

$$\frac{d[S]}{dt} = -I + k_0[S^*] + k_2[S^+][A^-] + k_3[S^+] \equiv P \tag{15}$$

$$\frac{d[A]}{dt} = -k_1[S^*][A] + k_2[S^+][A^-] + k_4[A^-] \equiv Q \tag{16}$$

where

$$I = I_0\{1 - \exp(-\epsilon l[S])\} \tag{17}$$

The derivatives in eqn. (12) which involve the flux, namely M_S and P_S, then become

$$M_S = I'$$

$$P_S = -I' - k_2(b - [A]_0) - k_3$$

where

$$I' = I_0 \epsilon l \exp(-\epsilon l [S]_0)$$

By making the formal identification $I' \rightarrow g$ (in effect by replacing one constant with another), it is evident that the conclusions of the foregoing analysis are unchanged.

3. Thermodynamic stability analysis of the steady state

A thermodynamic stability analysis of the steady state may be performed for two (simpler) mechanisms of special chemical interest. In ref. 6 the photoinduced redox process is represented as

$$S + A \underset{\Delta}{\overset{h\nu}{\rightleftarrows}} S^+ + A^- \tag{18}$$

with

$$S^+ + \tfrac{1}{2}H_2O \xrightarrow{k_3} S + H^+ + \tfrac{1}{4}O_2$$

$$A^- + H_2O \xrightarrow{k_4} A + OH^- + \tfrac{1}{2}H_2$$

One way of interpreting eqn. (18) is to assume that the concentration of species A is sufficiently large that the reaction to form the species S^+ and A^- occurs immediately on illumination of the system. Accordingly, we explore the consequences of assuming that reaction (18) is chemically (kinetically) controlled. In our notation eqn. (18) may be represented as

$$S + A \xrightarrow{g} S^+ + A^- \tag{19}$$

$$S^+ + A^- \xrightarrow{k_2} S + A \tag{20}$$

and the evolution equations for the system are

$$\frac{d[S]}{dt} = -g[S] + k_2[S^+][A^-] + k_3[S^+] \equiv P \tag{21}$$

$$= -\frac{d[S^+]}{dt}$$

$$\frac{d[A]}{dt} = -g[S] + k_2[S^+][A^-] + k_4[A^-] \equiv Q \tag{22}$$

$$= -\frac{d[A^-]}{dt}$$

The conservation conditions here are simply

$$[S] + [S^+] = a \tag{23a}$$

$$[A] + [A^-] = b \tag{23b}$$

We remark, first of all, that a linear stability analysis of the system, eqns. (21) and (22), may be performed using the techniques described in Section 2. In this case, however, the characteristic equation obtained for the system linearized about the (single) steady state is a quadratic equation

$$\lambda^2 - (P_S + Q_A)\lambda + (P_S Q_A - P_A Q_S) = 0$$

We then have that

$$\lambda_1 + \lambda_2 = -g - k_2(b - [A]_0) - k_3 - k_2(a - [S]_0) - k_4 < 0$$

and

$$\lambda_1\lambda_2 = gk_4 + k_2k_4(b - [A]_0) + k_3k_2(a - [S]_0) + k_3k_4 > 0$$

Noticing that

$$\begin{aligned}(\lambda_1 + \lambda_2)^2 - 4\lambda_1\lambda_2 = {} & \{g + k_2(b - [A]_0) + k_3 - k_2(a - [S]_0) - k_4\}^2 + \\ & + 4gk_2(a - [S]_0) + 4k_2^2(b - [A]_0)(a - [S]_0) \\ & > 0\end{aligned}$$

we conclude that (λ_1, λ_2) are both real and negative, thereby guaranteeing the asymptotic stability of the single steady state.

To carry out a Glansdorff–Prigogine thermodynamic stability analysis [12, 13], the excess entropy production is computed for the γ reactions in the system, *i.e.*

$$\frac{1}{2}\frac{\partial(\delta^2 S)}{\partial t} = \sum_\gamma \delta\omega_\gamma \delta\frac{A_\gamma}{T} \tag{24}$$

In this equation ω_γ is the reaction rate per unit volume for the γth reaction and A_γ is the affinity of reaction γ defined by

$$A_\gamma = -\sum_j \mu_j \nu_{j\gamma} = k_B T \log\left\{\frac{K^{eq}(T,\rho)}{\prod_j \rho_j^{\nu_{j\gamma}}}\right\}$$

In this last expression $K^{eq}(T,\rho)$ is the equilibrium constant, ρ_j is the concentration of reactant j, $\nu_{j\gamma}$ is the attendant stoichiometric coefficient and $k_B T$ is Boltzmann's constant times the temperature. In the problem under study

$$\frac{A_1}{T} = k_B \log\left(\frac{g[S]}{k_2[S^+][A^-]}\right) \qquad \omega_1 = g[S] - k_2[S^+][A^-]$$

$$\frac{A_2}{T} = k_B \log\left(\frac{k_3[S^+]}{k_{-3}[S]}\right) \qquad \omega_2 = k_3[S^+] - k_{-3}[S]$$

$$\frac{A_3}{T} = k_B \log\left(\frac{k_4[A^-]}{k_{-4}[A]}\right) \qquad \omega_3 = k_4[A^-] - k_{-4}[A]$$

In these expressions we have introduced (formally) the reverse rate constants k_{-3} and k_{-4}; however, under the conditions of the experiment, terms in ω_2 and ω_3 which are scaled by k_{-3} and k_{-4} may be suppressed. Making use of the conservation conditions, and computing the variations $\delta\omega_\gamma$ and $\delta(A_\gamma/T)$, eqn. (24) becomes

$$\frac{1}{2k_B}\frac{\partial(\delta^2 S)}{\partial t} = \left\{\frac{k_2(a-[S]_0)}{b-[A]_0} + \frac{k_4}{b-[A]_0} + \frac{k_4}{[A]_0}\right\}(\delta[A])^2 +$$

$$+ \left[\left(\frac{1}{[S]_0} + \frac{1}{a-[S]_0}\right)\{g + k_2(b-[A]_0)\} +\right.$$

$$\left. + \frac{k_3}{a-[S]_0} + \frac{k_3}{[S]_0}\right](\delta[S])^2 +$$

$$+ \left[\left(\frac{1}{[S]_0} + \frac{1}{a-[S]_0}\right) k_2(a-[S]_0) + \frac{1}{b-[A]_0} \times\right.$$

$$\left. \times \{g + k_2(b-[A]_0)\}\right]\delta[A]\,\delta[S]$$

Under steady state conditions the right-hand sides of eqns. (21) and (22) vanish and the following relations pertain:

$$b - [A]_0 = \frac{k_3}{k_4}(a - [S]_0)$$

$$g = \frac{1}{[S]_0}\left\{k_2\frac{k_3}{k_4}(a-[S]_0)^2 + k_3(a-[S]_0)\right\}$$

Using these relations the coefficients of $(\delta[A])^2$, $(\delta[S])^2$ and $\delta[A]\,\delta[S]$ may be simplified and in fact it is found that

$$\{\text{coefficient}(\delta[A]\,\delta[S])\}^2 - (4)\text{coefficient}(\delta[A])^2\text{coefficient}(\delta[S])^2$$

$$= -\left[\frac{a+[S]_0}{[S]_0(a-[S]_0)}\left\{\frac{4k_2a}{[S]_0} + \frac{k_4}{[S]_0} + \frac{2k_4a}{[S]_0(a-[S]_0)}\right\} +\right.$$

$$\left. + \frac{k_4}{[A]_0}\left\{\frac{k_2k_3}{k_4}\frac{a^2}{[S]_0^2} + \frac{k_3a^2}{[S]_0^2(a-[S]_0)}\right\}\right]$$

$$< 0$$

Given this inequality, and since it is found that

$$\text{coefficient}(\delta[A])^2 > 0$$

and

$$\text{coefficient}(\delta[S])^2 > 0$$

we may conclude, regardless of the sign of the variations $\delta[A]$ and $\delta[S]$, that

$$\frac{1}{2k_B}\frac{\partial(\delta^2 S)}{\partial t} > 0$$

The sign of the inequality of the excess entropy production ensures the stability of the steady state, a conclusion which complements the result obtained in the linear stability analysis.

A second limiting mechanism, the analysis of which leads to valuable insights, is one in which the possible consequences of diffusion are considered. Given a constant system illumination, we argue that the reactants S and A are present in concentrations sufficiently dilute that a finite time is required for migration and subsequent reaction, *i.e.* we consider the consequence of assuming that the forward reaction of eqn. (18) is diffusion controlled. One way of formulating this possibility is to write

$$S + A \underset{k_2}{\overset{k_1}{\rightleftharpoons}} S^+ + A^- \tag{25}$$

where k_1 is considered to be a typical second-order rate constant. More precisely, we assume that illumination produces a long-lived intermediate state S^* and that the rate-determining step in the interaction of S with A is governed by the time required for diffusion and is modeled by the rate constant k_1. The kinetic equations in this case (eqn. (25) together with the hydrogen and oxygen evolution reactions) are

$$\frac{d[S]}{dt} = -k_1[S][A] + k_2[S^+][A^-] + k_3[S^+] \equiv P \tag{26}$$

$$= -\frac{d[S^+]}{dt}$$

$$\frac{d[A]}{dt} = -k_1[S][A] + k_2[S^+][A^-] + k_3[A^-] \equiv Q \tag{27}$$

$$= -\frac{d[A^-]}{dt}$$

where the conservation conditions are specified again by eqns. (23). It can be shown that the system, eqns. (26) and (27), admits a single steady state and a linear stability analysis leads to the following expression for the sum and product of the two eigenvalues of the problem:

$$\lambda_1 + \lambda_2 = -k_1[A]_0 - k_2(b - [A]_0) - k_3 - k_1[S]_0 - k_2(a - [S]_0) - k_4 < 0$$

and

$$\lambda_1\lambda_2 = k_4\{k_1[A]_0 + k_2(b - [A]_0)\} + k_3\{k_1[S]_0 + k_2(a - [S]_0)\} + k_3k_4 > 0$$

Accordingly, we must have

$$(\lambda_1 + \lambda_2)^2 - 4\lambda_1\lambda_2 > 0$$

which, in turn, means that the two eigenvalues λ_1 and λ_2 must be real and negative. Thus, for this (diffusion-limiting) mechanism the results of the linear stability analysis predict the asymptotic stability of the (eventual) steady state realized on system illumination.

A thermodynamic stability analysis of this mechanism, based on eqn. (24) for the excess entropy production, can also be carried out. Here it is found that

$$\begin{aligned}\frac{1}{2k_B}\frac{\partial(\delta^2 S)}{\partial t} = &\left[\left(\frac{1}{[A]_0} + \frac{1}{b-[A]_0}\right)\{k_1[S]_0 + k_2(a-[S]_0)\} + \right.\\ &\left. + k_4\left(\frac{1}{b-[A]_0} + \frac{1}{[A]_0}\right)\right](\delta[A])^2 +\\ &+\left[\left(\frac{1}{[S]_0} + \frac{1}{a-[S]_0}\right)\{k_1[A]_0 + k_2(b-[A]_0)\} + \right.\\ &\left. + k_3\left(\frac{1}{a-[S]_0} + \frac{1}{[S]_0}\right)\right](\delta[S])^2 +\\ &+\left[\left(\frac{1}{[A]_0} + \frac{1}{b-[A]_0}\right)\{k_1[A]_0 + k_2(b-[A]_0)\} + \right.\\ &+\left(\frac{1}{[S]_0} + \frac{1}{a-[S]_0}\right)\times\\ &\left.\times\{k_1[S]_0 + k_2(a-[S]_0)\}\right]\delta[A]\,\delta[S]\end{aligned}$$

By inspection it is seen that the coefficients of the terms $(\delta[A])^2$, $(\delta[S])^2$ and $\delta[A]\,\delta[S]$ are all positive. The conservation conditions and the steady state condition may be used to simplify the algebraic structure of these coefficients, and it is found that

$$\{\text{coefficient}(\delta[A]\,\delta[S])\}^2 - (4)\text{coefficient}(\delta[A])^2\text{coefficient}(\delta[S])^2 < 0$$

This inequality guarantees that

$$\frac{1}{2k_B}\frac{\partial(\delta^2 S)}{\partial t} > 0$$

which, in turn, ensures thermodynamic stability of the single steady state of the diffusion-controlled process (namely eqn. (25) and the hydrogen and oxygen evolution equations).

The results obtained in this section may be compared with those reported in Section 2 which pertain to the more general mechanism, eqns.

(1a) - (1e). What we have found is that, if the general mechanism is simplified by assuming that the reaction

$$S + A \underset{\Delta}{\overset{h\nu}{\rightleftharpoons}} S^+ + A^-$$

is either chemically controlled or diffusion controlled, the consequent steady state of the system is asymptotically stable, a conclusion which is supported both by a linear stability analysis and by a Glansdorff–Prigogine thermodynamic stability analysis. In contrast, a linear stability analysis of the full mechanism (I) suggests two possibilities.

(1) As is found in the simpler mechanisms discussed in this section, the eventual steady state is asymptotically stable with small perturbations from that state rectified by a monotonic evolution back to the steady state.

(2) The second possibility uncovered in the study of mechanism (I) was that, although the eventual steady state is asymptotically stable, small perturbations of the system away from this steady state may be rectified by an oscillatory return to the steady state.

Clearly it is of interest to determine which of these two possibilities is realized in the water cleavage system under study in this paper. Such a determination can be made by carrying out a full-scale numerical analysis of the dynamical system described by eqns. (1a) - (1e) using the lifetime and rate constant data already available in the literature. The results of these simulations will be described in the following section.

4. Dynamics of the cyclic water cleavage reaction

4.1. Specification of kinetic and system parameters

In this section we review briefly the rate constant data available for a systematic numerical study of mechanism (I); in our simulations we shall study both the large-scale dynamics of mechanism (I) as well as the stability of the eventual steady state. We specify first the rate constants k_i ($i = 0, 1, 2, 3, 4$) (see eqns. (1a) - (1e)) and we then discuss the representation of the radiation flux term.

From the work of Navon and Sutin [16] we know that irradiation of $Ru(bipy)_3^{2+}$ with light below 560 nm results in the formation of a charge transfer excited state [$^*Ru(bipy)_3^{2+}$] of relatively long lifetime, *i.e.* $\tau = 0.6\ \mu s$ in water at 25 °C. Using this information we set the rate constant k_0 of luminescence decay in the absence of quencher to be $k_0 = 1.67 \times 10^6\ s^{-1}$. The oxidative quenching process (in particular, the reduction of MV^{2+} in water) has been estimated by Brugger and Grätzel [17] to occur with a specific rate $k_1 = (2) \times 10^8\ M^{-1}\ s^{-1}$. They have also reported that the back reaction between MV^+ and $Ru(bipy)_3^{3+}$ in water can occur with a rate of $k_2 = 2.4 \times 10^9\ M^{-1}\ s^{-1}$. From the work of Creutz and Sutin [18] the dioxygen yield is known to be a sharp function of pH, *e.g.* at low pH (3 - 4.8) $Ru(bipy)_3^{3+}$ is reduced to $Ru(bipy)_3^{2+}$ with a first-order rate constant

$k_3 = (1.41 \pm 0.04) \times 10^{-4}$ s^{-1} (at 25 °C, ionic strength μ = 1.00 M and sodium sulfate buffer); this is the relevant rate constant for our simulations inasmuch as a pH of 4.7 is specified in the experiment described in ref. 10. Finally, in the dihydrogen production step Kiwi [19] has reported a first-order rate constant of 0.14×10^3 s^{-1} at a concentration of platinum catalyst of 10^{-4} M (where, specifically, the platinum is stabilized in the colloidal state via polyvinyl alcohol (PVA)); in the Pt–PVA system, at a concentration of platinum catalyst of 12.5×10^{-4} M (the highest concentration of platinum employed) the rate constant $k_4 = 5.7 \times 10^{+4}$ s^{-1}.

As has been pointed out previously [19], the kinetic effect of the platinum microelectrode on the dihydrogen production step is remarkable; a 12-fold increase in the platinum content of the colloid enhances the catalytic activity by a factor of approximately 600. It is of considerable interest to examine the consequences of this apparent enhancement of the kinetic step (eqn. (1e)) on the overall dynamics and stability of the eventual steady state. To this end we identify a kinetic enhancement parameter N which scales the power of ten by which the presence of the platinum microelectrode influences the rate k_4; in particular, we write

$$k_4 = (5.7 \times 10^{+4} \text{ s}^{-1}) \times 10^N$$

Thus, for example, setting $N = 0$ recovers the rate constant corresponding to the highest platinum content reported in ref. 19, whereas choosing $N = -3$ corresponds to the decrease in rate by (approximately) three orders of magnitude when the platinum content of the catalyst is suppressed by a factor of about 12. A similar sort of scheme can be adopted to assess (via simulation) the kinetic enhancement of dioxygen production in the presence of an RuO_2 microelectrode, one component of the system identified in ref. 10. Here the only available information is the rate constant k_3 in the absence of catalyst; however, we can write

$$k_3 = (1.41 \times 10^{-4} \text{ s}^{-1}) \times 10^M$$

and we can then explore the consequences on the dynamics for different choices of M; setting $M = 0$ corresponds to the uncatalyzed system, but choices $M > 0$ simulate the role of the RuO_2 microelectrode catalyst. To assess the combined role of the platinum and RuO_2 microelectrodes on the (optimal) rates of production of hydrogen and oxygen via the cyclic mechanism reported in ref. 10, we undertook a numerical study of mechanism (I) for a number of settings of the kinetic enhancement parameters [M, N]; these studies will be reported in the following sections.

To complete the specification of the parameters of model (I), we consider now the radiation flux term. Two sorts of radiation sources were employed in the Lausanne experiments [10, 20] and will be considered here, namely a projector (tungsten) light and a xenon lamp. As displayed in ref. 21, the light intensity I_0 of a 100 W tungsten lamp between 400 and 800 nm is sensibly approximated by a gaussian curve with a maximum intensity of 4.5×10^{-7} einsteins s^{-1} sr^{-1} at 620 nm; we assign

$$I_0 = \frac{SW}{V}(4.5 \times 10^{-9})\exp\left\{-\frac{(\lambda - 620)^2}{14\,000}\right\}\text{einsteins s}^{-1}\text{ l}^{-1} \quad (28)$$

where W is the power of the source (in watts), V is the volume (in liters) of sample illuminated and S is the steradian specification; the calculations reported in the following section for the tungsten source were carried out for two different power ratings (W = 250 W and W = 1000 W), the given experimental solution volume and a geometry specified by setting S = 1 sr. For the xenon lamp the data reported in ref. 21 suggest a gaussian representation of the incident intensity I_0 of light of the form

$$I_0 = \frac{SW}{V}(4.86 \times 10^{-9})\exp\left\{-\frac{(\lambda - 550)^2}{12\,000}\right\}\text{einsteins s}^{-1}\text{ l}^{-1} \quad (29)$$

The calculations in Section 5 for the xenon source were performed for one power setting (W = 450 W) but for two different steradian settings, S = 1 sr and S = 3.5 sr. In all calculations the path length l of the incident light is taken to be half the diameter of the cell or flask; to provide a basis for comparison all calculations were normalized initially to a sample volume of 250 ml.

To complete the full Beer's law specification of the absorbed light intensity I where

$$I = I_0\{1 - \exp(-\epsilon l[\text{S}])\} \quad (30)$$

we must take into account the fact that the extinction coefficient ϵ of $Ru(bipy)_3^{2+}$ has a pronounced wavelength dependence [22] with a maximum value of 15 000 at λ = 450 nm; accordingly, we parametrize the wavelength dependence of ϵ as a gaussian function of the form

$$\epsilon = 15\,000\exp\{(\lambda - 450)^2/1500\}\text{ cm}^{-1}\text{ M}^{-1} \quad (31)$$

In calculations based on eqn. (30), the full functional forms for I_0 (either eqn. (28) or eqn. (29)) and the extinction coefficient (eqn. (31)) were used. If, however, we were to analyze the Lausanne experiments [10, 20] using the linearized form of Beer's law, we would represent the absorption intensity I as

$$I = I_0\epsilon l[\text{S}] = g[\text{S}] \quad (32)$$

with the rate constant g for excitation of $Ru(bipy)_3^{2+}$ estimated by the average absorption intensity I_a over the wavelength range 400 - 700 nm for the projector lamp and over the wavelength range 450 - 700 nm for the xenon lamp. Since we can easily accommodate the full behavior (eqn. (30)) in our numerical simulations, use of eqn. (32) was not exploited.

4.2. Time evolution studies and stability of the steady state

The full system of kinetic equations corresponding to the overall mechanism (I) can be solved numerically, given the rate constant and flux data itemized in Section 4.1. To set the initial concentration of the species S and A, we specify the values given in the paper by Kalyanasundaram and Grätzel

[10]. In their work a solution containing 10^{-4} M $Ru(bipy)_3^{2+}$ and 2×10^{-3} M MV^{2+} at a pH of 4.7 was irradiated with a projector lamp in the presence of RuO_2 powder (50 mg per 150 ml), or colloidal RuO_2 (1 mg per 150 ml), and colloidal platinum (4.5 mg per 150 ml). In the studies using a xenon lamp the concentrations of $Ru(bipy)_3^{2+}$ and MV^{2+} were 10^{-4} M and 5×10^{-3} M respectively.

We draw the reader's attention to the evolution profiles displayed in Figs. 3 - 7 and the steady state concentrations [S*], [S^+] and [A^-] reported in Table 1. The steady state concentrations can be determined either from the long-time behavior of the evolution curves (Figs. 3 - 7) or from the solution of the steady state equations generated from system (I); the results of these two different calculations (see, for example, the data in Table 1) are in agreement to within the accuracy of numerical calculation (here, double precision). It can be mentioned that the rate constant data needed to specify system (I) span a range of values sufficiently different in magnitude that the underlying set of coupled differential equations is "stiff"; hence, the aforementioned consistency between calculated values of the steady state concentrations provides a useful check on the overall accuracy of the numerical methods.

The data displayed in Figs. 3 - 7 reveal that the concentrations of the species S*, S^+ and A^- change significantly over short time-scales and that the time required to achieve the steady state concentration (for S^+ and A^-) is a marked function of the catalytic activity of the system. The simplest behavior is exhibited by the species S*, the concentration of which is found to in-

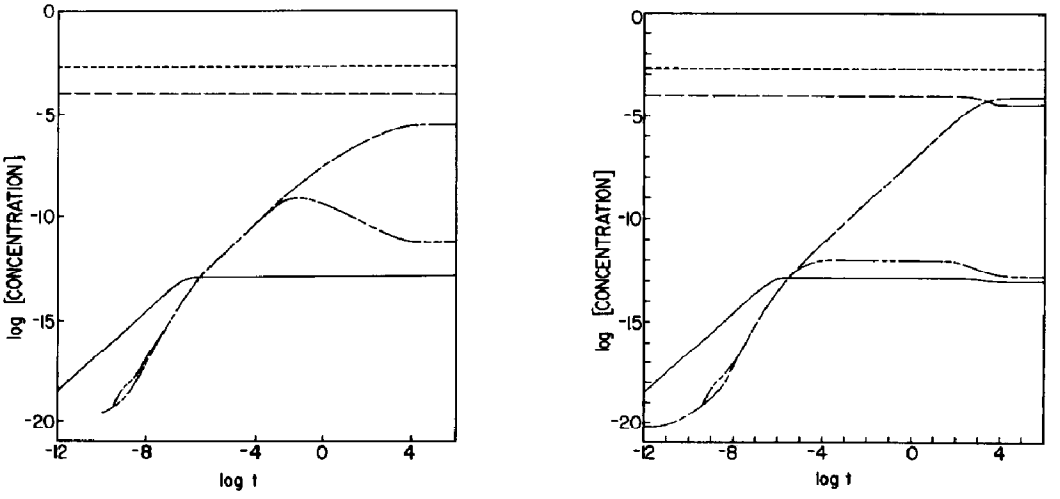

Fig. 3. Evolution profiles for the species S, S*, S^+, A and A^- corresponding to the choice $[M, N] = [0, -3]$ of enhancement exponents. We plot log(concentration) against log(time), with concentration in moles per liter and time in seconds: S, – – –, S; ———, S*; – · – · –, S^+; · · ·, A; – – – · – – – · – – –, A^-.

Fig. 4. Evolution profiles for the species S, S*, S^+, A and A^- corresponding to the choice $[M, N] = [0, 0]$ of enhancement exponents. (See caption to Fig. 3 for details.)

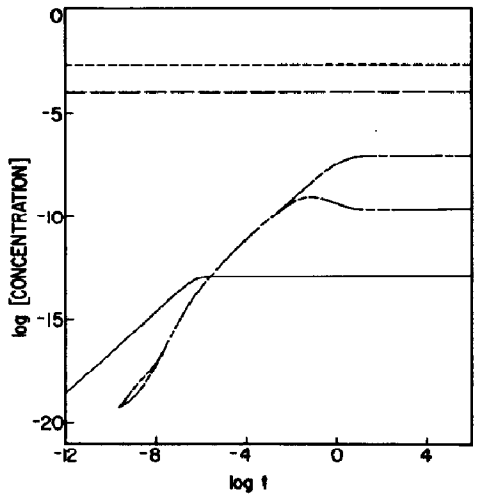

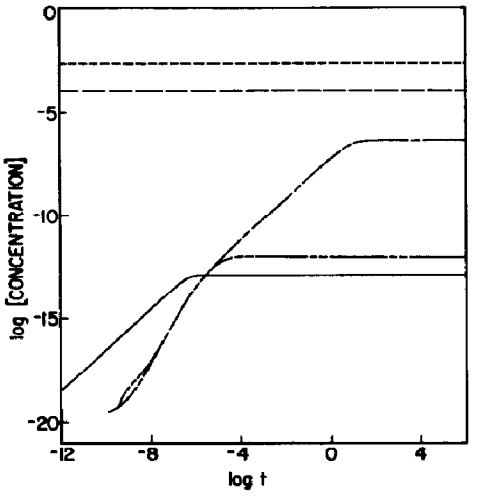

Fig. 5. Evolution profiles for the species S, S*, S^+, A and A^- corresponding to the choice $[M, N] = [3, -3]$ of enhancement exponents. (See caption to Fig. 3 for details.)

Fig. 6. Evolution profiles for the species S, S*, S^+, A and A^- corresponding to the choice $[M, N] = [3, 0]$ of enhancement exponents. (See caption to Fig. 3 for details.)

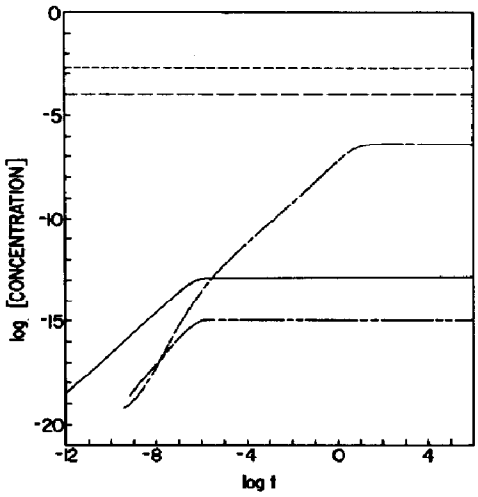

Fig. 7. Evolution profiles for the species S, S*, S^+, A and A^- corresponding to the choice $[M, N] = [3, 3]$ of enhancement exponents. (See caption to Fig. 3 for details.)

crease linearly (on the logarithmic plot) with time until, when $t \approx 10^{-6}$ s, the concentration [S*] stabilizes to the steady state value for all subsequent times. It should be noticed that both the steady state concentration and the effective stabilization time of the species S* are quite insensitive to the catalytic activity presumed to characterize reactions (1d) and (1e) in mechanism (I). In contrast, the steady state concentrations and effective stabilization times of the species S^+ and A^- are remarkably sensitive to the particular

TABLE 1

Steady state concentrations[a] and effective stabilization times[b] of the species S*, S^+ and A^- realized under catalytic conditions[c]

Species	*Enhancement exponents*[d]				
	[0, −3]	*[0, 0]*	*[3, −3]*	*[3, 0]*	*[3, 3]*
S*	0.132×10^{-12} (10^{-6})	0.864×10^{-13} (10^{-6})	0.134×10^{-12} (10^{-6})	0.134×10^{-12} (10^{-6})	0.134×10^{-12} (10^{-6})
S^+	0.298×10^{-5} (10^{+5})	0.653×10^{-4} (10^{+4})	0.839×10^{-7} (10^{+2})	0.374×10^{-6} (10^{+2})	0.380×10^{-6} (10^{+2})
A^-	0.737×10^{-11} (10^{+4})	0.162×10^{-12} (10^{+4})	0.208×10^{-9} (10^{+1})	0.925×10^{-12} (10^{-4})	0.940×10^{-15} (10^{-6})

[a] Primary entry in table with concentration reported in moles per liter.
[b] Secondary entry in table (in parentheses) with time in seconds reported to the nearest power of ten.
[c] The computations were performed given the following experimental conditions: a 250 W projector lamp illuminating a 250 ml flask (diameter, 8 cm) with a solid angle of 1 sr.
[d] See text for interpretation of the enhancement exponents [*M*, *N*].

settings of the enhancement exponents [*M*, *N*] and this behavior will now be discussed.

First of all, it is found that the times required to achieve the steady state for the species S^+ and A^- are dramatically shortened on increasing the catalytic activity. The effective stabilization times for S^+ drop by three orders of magnitude while those for A^- drop by ten orders of magnitude on enhancing the catalytic role of the microelectrode. Because the chemical network describing the cyclic mechanism (I) has non-linear terms which couple different equations in the set, it is both expected and found that enhancing reaction (1d) of S^+ also affects the stabilization times (and concentrations) of the species A^- (and vice versa). This common feature of synergetic systems represents a factor that might be exploited in the design of even more successful water cleavage systems.

The steady state concentrations of species S^+ and A^- change in a systematic way with increases in the values of the enhancement exponents [*M*, *N*]. Catalyzing only reaction (1e) of A^- causes an effective decrease in the steady state concentration of A^- and a concomitant increase in the steady state concentration of S^+, *e.g.* the concentration changes in Table 1 when [0, −3] → [0, 0] or when [3, −3] → [3, 0] should be noticed. A corresponding effect is noticed when the consequences of catalyzing (only) reaction (1d) of S^+ are examined; the steady state concentration $[S^+]$ is depressed whilst the steady state concentration $[A^-]$ increases (see, for example, the data for [0, −3] → [3, −3] or for [0, 0] → [3, 0]). These correlations can easily be understood by noticing that when, for example, the depletion of A^- via reaction (1e) is enhanced (thereby decreasing the

eventual steady state concentration of A^-), fewer molecules A^- are available for the (back) reaction of A^- with S^+ (via reaction (1c)), thereby leading to a net accumulation of S^+ and a resultant increase in the steady state concentration $[S^+]$.

The next point to be made follows from an examination of the dynamics displayed in Figs. 3 - 5. The "overshoots" in the concentration of A^- prior to the attainment of the eventual steady state should be noticed. Since the production of hydrogen is keyed to the net concentration of A^- (see Section 5), for a given setting of the enhancement exponents $[M, N]$ (*i.e.* for some final optimized microelectrode system) it may be desirable to run the system away from the steady state to realize the largest overall production of hydrogen. This can be done in a variety of ways, the simplest being to open up the system to mass transfer.

Finally, to return to the discussion presented in Sections 2 and 3, we have performed simulations to determine whether conditions can be realized such that, on perturbing the system away from its stable steady state, the system returns to the steady state via damped oscillations rather than via a simple monotonic decay. In our simulations we have found that damped oscillations are possible but only under conditions of impossibly high light flux conditions, *e.g.* for the catalytic situation [3, 3] a power of 0.15×10^{12} W is required to realize such non-monotonic behavior. Thus, we may conclude that the cyclic system (I) is not only asymptotically stable for all catalytic conditions and fluxes but also on perturbation the system regains its steady state exponentially fast.

5. Production of hydrogen and oxygen: results and discussion

The representative time evolution studies reported in Section 4.2 can be extended considerably and the behavior of system (I) under a variety of experimental conditions can be studied to infer optimal conditions for the production of oxygen and hydrogen. In Tables 2 - 4 we report the results of these simulations for two different visible light sources employed by Kalyanasundaram and Grätzel [10], the projector lamp and the xenon lamp. The simulations were performed using the appropriate expressions for I_0 for these two sources (eqn. (28) and eqn. (29) respectively) and the representation of the extinction coefficient ϵ given by eqn. (31), all in conjunction with the (non-linear) statement of Beer's law, eqn. (30). Calculations for two different power ratings (250 W and 1000 W) of the source were performed for the tungsten lamp, and calculations for two different solid angles (1 sr and 3.5 sr) were performed for the xenon lamp. Given the kinetic steps, eqns. (1d) and (1e), in the overall mechanism (I), we note that the production of oxygen and hydrogen in this cyclic system is keyed to the concentrations of S^+ and A^- respectively. Under steady state conditions we have

TABLE 2

Theoretical estimates of hydrogen and oxygen production under projector (tungsten) lamp illumination

Enhancement exponents [*M*, *N*]	*Power* (W)	$d[H_2]/dt$ (mol l^{-1} s^{-1})	$d[O_2]/dt$ (mol l^{-1} s^{-1})	$[H_2]$[a] (ml)	$[O_2]$[a] (ml)
[0, −3]	250	2.101×10^{-10}	1.050×10^{-10}	0.00762	0.00381
	1000	4.189×10^{-10}	2.095×10^{-10}	0.0152	0.00760
[1, −3]	250	6.608×10^{-10}	3.304×10^{-10}	0.0240	0.0120
	1000	1.328×10^{-9}	6.640×10^{-10}	0.0482	0.0241
[3, −3]	250	5.915×10^{-9}	2.958×10^{-9}	0.215	0.107
	1000	1.259×10^{-8}	6.294×10^{-9}	0.457	0.228
[6, −3]	250	2.640×10^{-8}	1.320×10^{-8}	0.958	0.479
	1000	1.012×10^{-7}	5.059×10^{-8}	3.67	1.836
[0, 0]	250	4.605×10^{-9}	2.303×10^{-9}	0.167	0.0836
	1000	6.312×10^{-9}	3.156×10^{-9}	0.229	0.115
[1, 0]	250	1.373×10^{-8}	6.865×10^{-9}	0.498	0.249
	1000	3.076×10^{-8}	1.538×10^{-8}	1.12	0.558
[3, 0]	250	2.637×10^{-8}	1.319×10^{-8}	0.957	0.479
	1000	1.007×10^{-7}	5.037×10^{-8}	3.65	1.828
[6, 0]	250	2.682×10^{-8}	1.341×10^{-8}	0.973	0.487
	1000	1.073×10^{-7}	5.364×10^{-8}	3.89	1.946

[a] In ref. 10 it was reported that illumination via a 250 W tungsten lamp for 3 h of a sample volume of 150 ml produced 0.6 ml of hydrogen and 0.3 ml of oxygen. Our estimates were computed for this irradiation time and sample volume.

TABLE 3

Theoretical estimates of hydrogen and oxygen production under xenon lamp illumination (1 sr)

Enhancement factors [*M*, *N*]	*Power* (W)	$d[H_2]/dt$ (mol l^{-1} s^{-1})	$d[O_2]/dt$ (mol l^{-1} s^{-1})	$[H_2]$[a] (ml)	$[O_2]$[a] (ml)
[0, −3]	450	6.368×10^{-10}	3.184×10^{-10}	0.0514	0.0257
[1, −3]	450	2.029×10^{-9}	1.015×10^{-9}	0.164	0.0818
[3, −3]	450	1.964×10^{-8}	9.819×10^{-9}	1.58	0.792
[6, −3]	450	2.201×10^{-7}	1.105×10^{-7}	17.7	8.91
[0, 0]	450	6.729×10^{-9}	3.354×10^{-9}	0.543	0.271
[1, 0]	450	4.486×10^{-8}	2.243×10^{-8}	3.62	1.81
[3, 0]	450	2.181×10^{-7}	1.095×10^{-7}	17.7	8.83
[6, 0]	450	2.501×10^{-7}	1.250×10^{-7}	20.2	10.1
[3, 3]	450	2.474×10^{-7}	1.237×10^{-7}	20.2	9.98
[6, 6]	450	2.502×10^{-7}	1.251×10^{-7}	20.2	10.1

[a] In ref. 20 it was reported that illumination for 1 h of a sample volume of 1 l produced 45 ml of hydrogen and 16 ml of oxygen. Our estimates were computed for this irradiation time and sample volume.

TABLE 4

Theoretical estimates of hydrogen and oxygen production under xenon lamp illumination (3.5 sr)

Enhancement exponents [*M*, *N*]	*Power* (W)	$d[H_2]/dt$ (mol l^{-1} s^{-1})	$d[O_2]/dt$ (mol l^{-1} s^{-1})	$[H_2]^a$ (ml)	$[O_2]^a$ (ml)
[0, −3]	450	1.175×10^{-9}	5.875×10^{-10}	0.0948	0.0474
[1, −3]	450	3.788×10^{-9}	1.894×10^{-9}	0.305	0.153
[3, −3]	450	3.743×10^{-8}	1.871×10^{-8}	3.02	1.51
[6, −3]	450	6.348×10^{-7}	3.174×10^{-7}	51.2	25.6
[0, 0]	450	6.958×10^{-9}	3.479×10^{-9}	0.561	0.281
[1, 0]	450	6.147×10^{-8}	3.074×10^{-8}	4.96	2.48
[3, 0]	450	6.206×10^{-7}	3.103×10^{-7}	50.0	25.0
[6, 0]	450	8.751×10^{-7}	4.375×10^{-7}	70.6	35.3
[3, 3]	450	8.407×10^{-7}	4.203×10^{-7}	67.8	33.9
[6, 6]	450	8.755×10^{-7}	4.378×10^{-7}	70.6	35.3

[a] In ref. 20 it was reported that illumination for 1 h of a sample volume of 1 l produced 45 ml of hydrogen and 16 ml of oxygen. Our estimates were computed for this irradiation time and sample volume.

$$\frac{d[O_2]}{dt} = \frac{1}{4} k_3 [S^+]_0$$

$$\frac{d[H_2]}{dt} = \frac{1}{2} k_4 [A^-]_0$$

where again we write

$$k_3 = (1.41 \times 10^{-4}\ s^{-1}) \times 10^M$$

$$k_4 = (5.7 \times 10^{+4}\ s^{-1}) \times 10^N$$

At this point, it is well to remind the reader of our interpretation of the enhancement exponents [*M*, *N*]. As is evident, the exponent *M* scales the power of ten by which the rate constant k_3 (governing the production of oxygen in reaction (1d)) is augmented by the presence of the RuO_2 catalyst; in our systems-theoretic approach, changing *M* from zero to some positive value allows us to ascertain the effect on the kinetics if the RuO_2 catalyst were to enhance the kinetic rate k_3 by *M* orders of magnitude. Similarly, the exponent *N* scales the power of ten by which the colloidally dispersed platinum catalyst enhances the rate k_4. As remarked earlier, Kiwi [19] has reported that nearly a threefold order-of-magnitude increase in the rate k_4 can be achieved, depending on the concentration of platinum present in the system. A lower bound on this catalytic activity is modeled in our approach by the exponent $N = -3$ whilst the "highest" rate reported by Kiwi is identified with the choice $N = 0$; for completeness, intermediate and even larger values of *N* are also considered in our simulations. In this way we can explore the possible consequences (*vis-à-vis* oxygen and hydrogen production)

of designing experimental systems of varying degrees of microelectrode catalytic activity.

To make a comparison with the Lausanne experiments [10], we recall that 0.6 ml of hydrogen and 0.3 ml of oxygen were produced via illumination of a 150 ml sample for 3 h with a 250 W projector lamp. Since kinetic enhancement of the rate k_3 due to the presence of RuO_2 is expected and given the "highest" value of k_4 reported by Kiwi, it is probable that the data listed in Table 2 for [1, 0] or possibly even [3, 0] would correspond most closely to the experimental situation. As is seen from Table 2, the actual experimental values reported in ref. 10 are bracketed by the numerical estimates generated for these two cases. We believe this lends support to the view that the cyclic water cleavage reaction discovered by Grätzel and coworkers is being modeled adequately via the chemical network eqns. (1a) - (1e). Further support for this view is given when the data reported by the Lausanne group [20] on the production of hydrogen and oxygen via illumination for 1 h with a 450 W xenon source are considered; a sample volume of 1 l yielded 45 ml of hydrogen and 16 ml of oxygen. Increasing the solid angle from 1 to 3.5 sr in our simulations shows that the estimated hydrogen and oxygen production corresponding to the enhancement exponents [1, 0] and [3, 0] once again bracket the experimental values reported in ref. 20. Given this agreement, we now go on to explore the consequences of changing [M, N] and the illumination in regimes other than those considered in the experimental studies cited here.

First of all, with respect to changing the power rating of the source, it is seen that a fourfold increase in wattage of the tungsten lamp produces an approximately twofold increase in the net production of hydrogen and oxygen in kinetic regimes where the rate enhancement (of k_3 and k_4 via the microelectrodes) is minimal. When the enhancement exponents [M, N] assume somewhat larger values, this fourfold increase in intensity leads to a threefold increase (approximately) in the production of hydrogen and oxygen. In other words, the cyclic water cleavage reaction (I) behaves as a typical synergetic system wherein the enhancement of one effect (namely the rates of reactions (1d) and (1e)) enhances the role of the other system parameters (here the illumination of the source). Secondly, as expected, the illumination of a larger solid angle leads to an increased production of hydrogen and oxygen (illustrated by the data reported for the xenon lamp) but, once again, the net enhancement is greater the greater the kinetic enhancement is. With respect to both these factors (*i.e.* the power rating of the source and the solid angle illuminated), the data reported in Tables 2 - 4 show that a plateau is reached with respect to the production of hydrogen and oxygen as the values of the exponents [M, N] are increased. The most significant improvements in the production of hydrogen and oxygen are realized on going from the uncatalyzed system [0, −3] to [3, 0], for example; increases to values of [M, N] larger than [3, 0] result only in "secondary" increases in the yield of hydrogen and oxygen. This information is encouraging with respect to the search for successful microelectrode systems; it would

certainly be disappointing if yields could be improved significantly only by finding catalytic systems which enhanced the rates k_3 and k_4 by many powers of ten. Conversely, the convergence in yields for the [3, 3] *versus* [6, 6] cases in Tables 3 and 4 suggests strongly that there is an effective upper bound on the yields that can be produced via the cyclic system (I) using a dispersed microelectrode catalyst system. Accordingly, the optimal efficiency of the cyclic system (I) can be assessed against other methods of light energy conversion (*e.g.* photogalvanic cells) and this point will be discussed in the following section.

6. Concluding remarks

In this paper we have explored analytically and numerically the stability and evolution of a possible model for the cyclic water cleavage system reported recently by Kalyanasundaram and Grätzel [10]. Considering first the stability of the (single) photostationary state, our analysis showed that, while the asymptotic stability of the steady state is guaranteed, on being subjected to a small perturbation the system can regain the steady state either monotonically or via damped oscillations. Our simulations then showed conclusively that the latter (theoretical) possibility can be dismissed inasmuch as the flux conditions required to elicit such a damped oscillatory response on perturbation are simply outside the regime of experimental possibility. At the same time, however, the evolution studies revealed the existence of "overshoots" and "undershoots" in the evolving concentrations, especially in regimes of suppressed catalytic activity, thereby suggesting that the efficiency of hydrogen and oxygen production might be amplified (in these regimes) by operating the system away from the photostationary state. By exploring systematically changes in the parameters of the model, specifically those which pertain to the system illumination (intensity and geometry) and kinetic enhancement (due to the dispersed microelectrode catalyst), it was found that the experimental yields of hydrogen and oxygen reported by the Lausanne group [10, 20] were bracketed by our theoretical estimates for reasonable choices of these parameters (see Section 5); moreover, the simulations pointed to the existence of an effective upper bound on the yields of hydrogen and oxygen attainable via mechanism (I).

The study presented in this paper complements earlier work [15] on the stability properties of photochemical mechanisms for photogalvanic cells. Taken together, the water cleavage system and the photogalvanic cell have certain (theoretical) features in common: each may be represented as a coupled chemical network driven by a flux of electromagnetic radiation and, as such, can be investigated using methods found to be successful in the analysis of synergetic systems in general. Having cast both problems within this common theoretical framework, it is of interest to consider the relative efficiency of these two energy storage–transfer systems. Put simply, for a given light energy input the effective energy conversion of the photogalvanic

cell (to electrical energy) *versus* that of the water cleavage system (to chemical energy) can be examined. While such estimates can be made almost at once given the underlying experimental evidence already in the literature, we believe it may be possible to place these estimates on a more microscopic footing. Recently we have presented [23] a detailed characterization and comparison of the electrostatic environment of charged microelectrodes *versus* planar electrodes, a study wherein effects due to dielectric saturation were taken explicitly into account. In particular, it was found that the behavior (namely reduced mean potential and attendant counter-ion distributions) exhibited by spherical charged organizates tends to converge to the behavior exhibited by a model for a planar electrified interface as the size of the spherical organizate increases. Although intuitively such behavior should be expected, the calculations showed that a charged constellation of metal (metal oxide) atoms begins to behave, electrostatically, like a miniature planar electrode (a microelectrode) when the effective diameter of the organizate is $d \geqslant 100$ Å. The estimates of the (average) sizes of the metal (metal oxide) microelectrodes utilized by Grätzel and coworkers fall in the range $d > 100$ Å, thereby indicating that the microelectrodes in their colloidal dispersion behave (locally at least) like "true" electrodes. This leads us to suggest that, although the photogalvanic system [2 - 4] and the cyclic water cleavage system [10] are superficially quite different, the field effects which control reaction and diffusion to the reactive surface may be quite similar in the two systems. Accordingly, we believe that an analysis of the photogalvanic cell and the water cleavage system along the lines of the present study, but incorporating field-induced diffusion, would lead to more reliable estimates of the relative efficiency of the two systems than can be obtained using simple mass action arguments to gauge the conversion of radiant energy into electrical and/or chemical energy. This study is in progress and will be reported in the near future.

Acknowledgments

This work was supported by the Office of Basic Energy Sciences of the U.S. Department of Energy. This is Document NDRL-2200 from the Notre Dame Radiation Laboratory.

References

1 G. Porter and M. D. Archer, *Interdiscip. Sci. Rev., 1* (1976) 119.
M. Calvin, *Photochem. Photobiol., 23* (1976) 425.
J. R. Bolton (ed.), *Solar Power and Fuels*, Academic Press, New York, 1977.
Proc. 4th Department of Energy Solar Photochemistry Res. Conf., Notre Dame, IN, June 1 - 4, 1980.
2 W. J. Albery, W. R. Bowen and M. D. Archer, *J. Photochem., 11* (1979) 15.
3 W. J. Albery, W. R. Bowen, M. D. Archer and M. I. Ferreira, *J. Photochem., 11* (1979) 27.

4 W. J. Albery and M. D. Archer, *Nature (London), 270* (1977) 399.
5 B. V. Koryakm, T. S. Dzhabiev and A. E. Shilov, *Dokl. Akad. Nauk S.S.S.R., 238* (1977) 620.
J. M. Lehn and J. P. Sauvage, *Nouv. J. Chim., 1* (1977) 449.
6 K. Kalyanasundaram, J. Kiwi and M. Grätzel, *Helv. Chim. Acta, 61* (1978) 2720.
7 A. Moradpour, E. Amouyal, P. Keller and H. Kagan, *Nouv. J. Chim., 2* (1978) 547.
8 R. O. Durham, W. J. Dressick and T. J. Meyer, *J. Chem. Soc., Chem. Commun.*, (1979) 381.
9 J. Kiwi and M. Grätzel, *Angew. Chem., 90* (1978) 900.
J. Kiwi and M. Grätzel, *Angew. Chem., Int. Edn. Engl., 17* (1978) 860; *18* (1979) 624.
J. Kiwi and M. Grätzel, *Chimia, 33* (1979) 289.
10 K. Kalyanasundaram and M. Grätzel, *Angew. Chem., Int. Edn. Engl., 18* (1979) 701.
11 A. Henglein, *Angew. Chem., Int. Edn. Engl., 18* (1979) 418.
A. Henglein, *J. Phys. Chem., 83* (1979) 2209.
12 P. Glansdorff and I. Prigogine, *Thermodynamic Theory of Structure, Stability and Fluctuations*, Interscience, New York, 1971.
13 G. Nicolis and I. Prigogine, *Self-organization in Non-equilibrium Systems*, Wiley, New York, 1977.
14 H. Haken, *Synergetics*, Springer, Berlin, 1977.
15 M. H. Dung and J. J. Kozak, *J. Photochem., 14* (1980) 205.
16 G. Navon and N. Sutin, *Inorg. Chem., 13* (1974) 2159.
17 P. A. Brugger and M. Grätzel, *J. Am. Chem. Soc., 102* (1980) 2461.
18 C. Creutz and N. Sutin, *Proc. Natl. Acad. Sci. U.S.A., 72* (1975) 2858.
19 J. Kiwi, *Isr. J. Chem., 18* (1979) 369.
20 J. Kiwi, E. Borgarello, E. Pelizzetti, M. Visca and M. Grätzel, *Angew. Chem., Int. Edn. Engl., 19* (1980) 646.
21 C. A. Parker, *Photoluminescence of Solutions*, Elsevier, Amsterdam, 1968.
22 J. N. Demas and G. A. Crosby, *J. Am. Chem. Soc., 93* (1971) 2841.
23 M. H. Dung, D. G. Knox and J. J. Kozak, *Ber. Bunsenges. Phys. Chem., 84* (1980) 789.